JOURNAL OF COMPUTATIONAL PHYSICS 94, 30–58 (1991)

Spectral Method Solution of the Stokes Equations on Nonstaggered Grids

MARK R. SCHUMACK AND WILLIAM W. SCHULTZ

Department of Mechanical Engineering and Applied Mechanics, University of Michigan, Ann Arbor, Michigan 48109

AND

JOHN P. BOYD

Department of Atmospheric, Oceanic, and Space Science, University of Michigan, Ann Arbor, Michigan 48109

Received June 16, 1989; revised December 28, 1989

The Stokes equations are solved using spectral methods with staggered and nonstaggered grids. Numerous ways to avoid the problem of spurious pressure modes are presented, including new techniques using the pseudospectral method and a method solving the weak form of the governing equations (a variation on the "spectral element" method developed by Patera). The pseudospectral methods using nonstaggered grids are simpler to implement and have comparable or better accuracy than the staggered grid formulations. Three test cases are presented: a formulation with an exact solution, a formulation with homogeneous boundary conditions, and the driven cavity problem. The solution accuracy is shown to be greatly improved for the driven cavity problem when the analytical solution of the singular flow behavior in the upper corners is separated from the computational solution.

1. INTRODUCTION

Spectral methods offer high accuracy and are promising tools for fluid dynamics problems requiring high resolution. When solving the equations governing incompressible flow in primitive variable form, however, the numerical solution can be polluted by spurious pressures (nontrivial null spaces in the matrix of the discrete problem). Researchers have avoided the spurious pressure problem by solving a Poisson equation for pressure [15]. A chief concern for the formulations involving a Poisson equation is the pressure boundary conditions [12, 15]. When the momentum and continuity equations are solved directly, i.e., without a Poisson equation for pressure, staggered grids [2, 4, 9, 10, 13, 16] are often employed to avoid spurious pressures. Staggered grids, however, complicate the programming and can also require the construction of particular solutions for inhomogeneous boundary conditions.

0021-9991/91 $3.00

In this paper, we show that there are a number of ways to avoid the use of staggered grids in solution of the Stokes equations without a Poisson equation for pressure. We use the pseudospectral method [6] and a method involving a weak form of the governing equations. The weak formulation is similar to the "spectral element" method as developed by Patera [14], Maday [9], and Ronquist [16]. Solution of the two-dimensional Stokes equations serves as a prerequisite for solution of the full three-dimensional Navier–Stokes equations.

2. Formulation

In this section, we describe the spectral methods we use to solve the Stokes equations. We present a number of new techniques that do not require the use of staggered grids, and we compare staggered and nonstaggered grid techniques for both the pseudospectral and weak formulations. Ten formulations are presented. To facilitate subsequent discussion and reference to the figures, each formulation is assigned a number (see below) and a symbol (see Table I).

We formulate and test the pseudospectral method in eight ways:

1. Nonstaggered grid, continuity applied on boundary [11]
2. Nonstaggered grid, normal momentum equation applied on boundary
3. Nonstaggered grid, pressure approximated with lower order polynmials than velocity

TABLE I

Legend for Formulations and Figures

Symbol	▽	×	•	■	△	◇	+	⧓	○	□
Formulation number	1	2	3	4	5	6	7	8	9	10
Number equations = number unknowns	•	•	•	•	•			•	•	•
Number equations > number unknowns						•	•			
Singular matrix	•				•					
Continuity applied on boundary	•						•			
x- and y-momentum equations applied on boundary							•			
Normal momentum equation applied on boundary		•								
Pressure and velocity of same order	•	•				•	•			
Pressure lower order than velocity			•	•	•			•	•	•
Number collocation points > number basis functions						•				
Nonstaggered grid	•	•	•			•	•	•	•	
Semi-staggered grid					•					•
Fully staggered grid				•						
Weak formulation									•	•
Strong formulation	•	•	•	•	•	•	•	•		
Chebyshev basis	•	•	•	•	•	•	•			
Legendre basis								•	•	•
Lagrangian interpolants for velocity and pressure										•
Lagrangian interpolants for v, Legendre expansion for p									•	
Reference	[11]			[2]	[10]	[18]				[9]

4. Fully-staggered grid (continuity, x-momentum, and y-momentum equations satisfied on three different sets of grid points) [2]

5. Semi-staggered grid (continuity and momentum equations satisfied on two different sets of grid points) [10]

6. Nonstaggered grid, overdetermined system formed by increasing the number of collocation points

7. Nonstaggered grid, overdetermined system formed by satisfying continuity and both the x- and y-momentum equations on the boundary.

We use Chebyshev polynomials as the basis set for the pseudospectral formulations listed above. To judge the effect of this choice, we solve one of our test problems using the pseudospectral method with a Legendre basis:

8. Nonstaggered grid, pressure approximated with lower order polynomials than velocity–Legendre basis.

Then, turning to the weak formulation, we solve the problem in two ways:

9. Nonstaggered grid, pressure approximated with a standard orthogonal polynomial expansion of lower order than the polynomials used for velocity

10. Semi-staggered grid, pressure approximated with standard Lagrangian interpolants of lower order than those used for velocity [9, 16].

Legendre polynomials are used for the weak formulation. A Legendre basis results in a more computationally efficient procedure than a Chebyshev basis [14] due to the type of quadrature employed, as described by Ronquist [17] (see Sect. 2.2).

We solve three test problems: (1) a form for which an exact solution exists, (2) a form with homogeneous boundary conditions, and (3) the driven cavity problem. For all the formulations presented here, we solve the problem on a single-element rectangular domain, $-1 \leqslant x, y \leqslant 1$. (However, both weak formulations have been successfully extended to multi-element rectilinear domains; we briefly present the multi-element results in Section 4.) All of our matrix equations are solved with direct (as opposed to iterative) solvers. However, we briefly discuss the implementation of iterative solvers in Section 5.

In the remainder of this paper, we use the term "Lagrangian interpolant" to define an interpolating polynomial $P_i(x)$ such that

$$P_i(x_j) = \delta_{ij}. \tag{1}$$

We present results for the driven cavity problem to show how the accuracy of spectral methods is affected by the presence of corner singularities. We find that the solution is greatly improved when the singularity is removed by separating the analytical form of the singularity from the computational solution.

2.1. *Pseudospectral Method*

The unknowns in the pseudospectral method are expanded as products of orthogonal polynomials:

$$g = \sum_{n=0}^{N} \sum_{m=0}^{M} g_{nm} T_n(x) T_m(y). \tag{2}$$

Here we have used Chebyshev polynomials, denoted by $T_n(x)$. Later we introduce a formulation using Legendre polynomials. The differential equations are satisfied at a particular set of collocation points and boundary conditions are enforced to determine the unknown coefficients g_{nm}. Depending on the number of collocation points and the boundary conditions, the resulting system of linear equations is either determined, overdetermined, or singular.

The Stokes equations are as follows:

$$\nabla^2 \mathbf{u} - \nabla p = -\mathbf{f} \tag{3}$$

$$\nabla \cdot \mathbf{u} = 0. \tag{4}$$

The forcing function $\mathbf{f}$ is known. Expanding the velocity $\mathbf{u} = (u, v)$ and pressure p with the same truncation gives the representation

$$u = \sum_{n=0}^{N} \sum_{m=0}^{N} u_{nm} T_n(x) T_m(y) \tag{5}$$

$$v = \sum_{n=0}^{N} \sum_{m=0}^{N} v_{nm} T_n(x) T_m(y) \tag{6}$$

and

$$p = \sum_{n=0}^{N} \sum_{m=0}^{N} p_{nm} T_n(x) T_m(y). \tag{7}$$

For the rectangular domain $-1 \leqslant x, y \leqslant 1$ the $N+1$ extremum collocation points in each direction

$$x_j, y_j = -\cos \pi j/N, \qquad 0 \leqslant j \leqslant N, \tag{8}$$

give $(N+1)^2$ points to determine the $3 \times (N+1)^2$ unknown coefficients. Applying the momentum and continuity equations (3) and (4) at the interior collocation points yields $3 \times (N-1)^2$ equations, leaving $12N$ equations to fully determine the system. Applying the two velocity boundary conditions at each boundary node yields $8N$ equations (see Section 3 for a discussion of a multivalued velocity in the corners, as in the driven cavity problem). We could obtain the additional $4N$ equations by applying continuity on the boundary [11] (formulation 1, denoted by ∇), but the resulting system is singular; i.e., spurious pressure modes exist (see below

for a characterization of the spurious modes). The application of one component of the momentum equation at the boundary (with suitable treatment at the corners) will also supply the needed $4N$ equations. Applying the normal momentum equation on the boundary leads to a determined system (formulation 2, denoted by $\times$); i.e., we satisfy

$$\partial p/\partial x = \nabla^2 u + f_x \tag{9}$$

on the boundaries at $x = -1$ and $x = 1$, and

$$\partial p/\partial y = \nabla^2 v + f_y \tag{10}$$

on the boundaries at $y = -1$ and $y = 1$. Here, the subscripts x and y denote components of the x- and y-momentum equations. In the corners, we obtain a condition by taking the divergence of the momentum equation. Using $\nabla \cdot \mathbf{u} = \mathbf{0}$ leads to

$$\nabla^2 p = \nabla \cdot \mathbf{f}. \tag{11}$$

Application of the tangential momentum equation on the boundary leads to a singular matrix (see below).

Another way to obtain a determined system is to approximate pressure with a truncation of two less than for velocity in each direction (formulation 3, denoted by $\bullet$):

$$p = \sum_{n=0}^{N-2} \sum_{m=0}^{N-2} p_{nm} T_n(x)\, T_m(y). \tag{12}$$

Satisfying the differential equation at the interior collocation points and enforcing the velocity boundary conditions results in a determined system.

Staggered grids have also been employed to deal with the spurious pressure problem. The staggered grids presented here use two sets of collocation points, the extrema grid (8) and the set of N points in each direction:

$$\tilde{x}_j,\ \tilde{y}_j = -\cos \pi(2j+1)/2N, \qquad 0 \leqslant j \leqslant N-1. \tag{13}$$

Note that the collocation points (13) are the roots of $T_N(x)$. The extrema grid (8) includes the endpoints for a total of $N+1$ collocation points in each direction, and the roots grid (13) defines N interior collocation points in each direction. We approximate u and v as

$$u = \sum_{n=0}^{N-2} \sum_{m=0}^{N-1} u_{nm} T_n(x)\, T_m(y)(1-x^2)(1-y^2) \tag{14}$$

$$v = \sum_{n=0}^{N-1} \sum_{m=0}^{N-2} v_{nm} T_n(x)\, T_m(y)(1-x^2)(1-y^2) \tag{15}$$

(which satisfy homogeneous boundary conditions), and p as

$$p = \sum_{n=0}^{N-1} \sum_{m=0}^{N-1} p_{nm} T_n(x) T_m(y). \tag{16}$$

Satisfying the x-momentum equation at points $(x_i, \tilde{y}_j)$, the y-momentum equation at points $(\tilde{x}_j, y_i)$, and continuity at $(\tilde{x}_j, \tilde{y}_k)$ for $1 \leqslant i \leqslant N-1$, $0 \leqslant j \leqslant N-1$, and $0 \leqslant k \leqslant N-1$, results in a determined and nonsingular linear system [2] (formulation 4, denoted by ■). Note that this formulation is restricted to problems with homogeneous boundary conditions. Similar formulations could be devised for inhomogeneous boundary conditions [6] but are complicated by the separate construction of particular solutions.

The semi-staggered formulation (formulation 5, denoted by △) approximates u and v as in (5) and (6) but p as in (16). Then the x- and y-momentum equations are satisfied on the interior points of the extrema grid (8) and continuity is satisfied on the roots grid (13). This formulation results in a singular system with spurious pressure modes, as will be seen.

We can also consider the least-squares solution of overdetermined systems. We show that there are numerous ways to overdetermine the system and that in many cases overdetermination improves the accuracy.

The simplest way to overdetermine the system is to increase the number of collocation points $M > N$ such that the collocation points are

$$x_j, y_j = -\cos \pi j/M, \qquad 0 \leqslant j \leqslant M. \tag{17}$$

If $M = N+1$ is chosen, the resulting system has more equations than unknowns but is singular (see below). To obtain a non-singular system, $M > N+1$. Here, we choose $M = N+2$ (formulation 6, denoted by ◇). The solution of overdetermined systems with the least-squares method depends on the magnitude of the rows of the matrix. Therefore, we normalize each row and corresponding right-hand-side entry such that the largest entry in each row has an absolute value of unity. We can also weight certain rows by multiplying the entire row and corresponding right-hand-side entry by a constant, if desired. By weighting the boundary condition rows more than other rows, we can satisfy the prescribed boundary conditions to any desired accuracy, but the degree to which the differential equation is satisfied at the collocation points will be compromised. For our calculations, we simply assign every normalized row a weight of unity. One can also increase the number of collocation points for one of the determined formulations (above) to overdetermine the system. We have found that this method often leads to slightly better results if the overdetermination is not too great.

Another way to overdetermine the system is to apply continuity and both momentum equations at the boundary (formulation 7, denoted by +).

We also solve one test problem using Legendre polynomials instead of Chebyshev polynomials in (5), (6), and (12) to gauge the effect of basis choice (formulation 8, denoted by *).

In all the pseudospectral methods discussed above, we set the constant pressure mode by adding an equation specifying $p_{00}=0$. This additional equation necessitates using a least-squares solver for even the determined systems. Alternatively, we have solved the determined systems by replacing one continuity equation with an equation specifying $p_{00}=0$ [19]—this substitution maintains an equal number of equations and unknowns—and results were nearly identical to the case with one additional equation.

Characterization of spurious pressure modes. Spurious pressure modes for spectral approximations have been described by Bernardi, Maday, and Metivet [3] (for a Legendre basis), and Bernardi, Canuto, and Maday [5] (for a Chebyshev basis). We discuss the Chebyshev basis here. The spurious pressure modes are defined as follows. If p is a solution to the Stokes equations (3) and (4), and p_H exists such that its x- and y-derivatives vanish at all collocation points where the momentum equations are satisfied, then $(p+p_H)$ is also a solution. The quantity p_H is a spurious pressure solution. It should be noted that derivatives of the constant mode $T_0(x)\,T_0(y)$ vanish for all (x, y). Therefore, multiples of this mode are not spurious solutions, but a multiple of this mode must be specified at some point (x, y) for (3) and (4) to have a unique pressure solution.

For the formulation where continuity is applied at the boundary ($\triangledown$), the spurious pressure solutions are characterized by any multiples of the three modes

$$T_i(x)\,T_j(y), \qquad i, j=0, N;\ i=j\neq 0, \tag{18}$$

and by four linear combinations of modes:

$$\sum_{\text{odd}}\sum_{\text{odd}} c_{ij}T_i(x)\,T_j(y), \qquad \sum_{\text{even}}\sum_{\text{even}} c_{ij}T_i(x)\,T_j(y),$$

$$\sum_{\text{odd}}\sum_{\text{even}} c_{ij}T_i(x)\,T_j(y), \qquad \sum_{\text{even}}\sum_{\text{odd}} c_{ij}T_i(x)\,T_j(y).$$

For the semi-staggered grid formulation ($\triangle$), one linear combination of modes resulting in a spurious pressure solution exists. It is characterized by a linear combination of modes whose parity is opposite that of the truncation N, i.e.,

$$\sum_{\text{odd}}\sum_{\text{odd}} c_{ij}T_i(x)\,T_j(y) \tag{19}$$

if N is even, and the summations are over even indices i, j if N is odd.

When the system is overdetermined by increasing the number of collocation points, the formulation is singular for $M=N+1$ with one spurious pressure solution. This spurious solution arises in the same way as that for the semi-staggered formulation: pressure is approximated with a truncation of one less than the polynomial defining the collocation grid.

We did not characterize the spurious pressure solutions for the case where the

tangential momentum equation is applied on the boundary, but we can easily show that the three modes described by (18) will not be eliminated. For example, at $y = \pm 1$, (18) becomes

$$\pm T_i(x), \qquad i = 0, N, \tag{20}$$

whose x-derivative is always zero (except in corners). On the other hand, when we apply the normal momentum equation at $y = \pm 1$ (formulation denoted by $\times$), the y-derivative of (18) for $j = N$ does not vanish (it is equal to $\pm N^2$).

2.2. *Weak Formulation*

In this section we apply the method developed in [9, 16], with some variations to eliminate the need for a staggered grid.

By approximating pressure in a conventional orthogonal polynomial expansion (in contrast to a typical Lagrangian interpolant given by (1)) with an order two less than that for velocity, we avoid a staggered grid. Ronquist [17] compares Chebyshev and Legendre expansion methods and shows that while the accuracy of the two is comparable, the operation count for Chebyshev methods "is not competitive with Legendre techniques for time-dependent geometries or iterative solution procedures." The Chebyshev method [14] utilizes exact integration formulas, and the inner products are defined with a weight of unity. Because the inner products are not defined with the usual Chebyshev weight function $(1-x^2)^{-1/2}$, certain simplifications resulting from Gaussian quadrature cannot be implemented. The Gaussian quadrature in the Legendre method, however, uses a weighting of unity; therefore, we use a Legendre basis to take advantage of simplifications that result in a reduced operation count (at the expense, however, of exact integration).

The development we present here is for a single rectangular domain. In our method, we approximate the velocity components as

$$u = \sum_{n=0}^{N} \sum_{m=0}^{N} u_{nm} h_n(x)\, h_m(y) \tag{21}$$

$$v = \sum_{n=0}^{N} \sum_{m=0}^{N} v_{nm} h_n(x)\, h_m(y) \tag{22}$$

and pressure as

$$p = \sum_{n=0}^{N-2} \sum_{m=0}^{N-2} p_{nm} L_n(x)\, L_m(y). \tag{23}$$

Here, the Lagrangian interpolants are defined by

$$h_j(x) = -\frac{(1-x^2)\, L'_N(x)}{N(N+1)\, L_N(x_j)(x-x_j)}. \tag{24}$$

These interpolants are derived by taking a Taylor series expansion about the roots

of $(1-x^2)\,L'_N(x)$ [6, 16]. The x_j in Eq. (24) are the roots of $(1-x^2)\,L'_N(x)$ (the roots of $L'_N(x)$ are not known in closed form). Note that these Lagrangian interpolants satisfy (1). The coefficients u_{nm} and v_{nm} are the velocity components at (x_n, y_m), but the p_{nm} are spectral coefficients, not the pressure values on the grid.

Now, we take inner products of the Stokes equations:

$$-\int_\Omega (\nabla^2 \mathbf{u})\cdot \mathbf{w}\, d\Omega + \int_\Omega \nabla p \cdot \mathbf{w}\, d\Omega = \int_\Omega \mathbf{f}\cdot \mathbf{w}\, d\Omega \tag{25}$$

$$-\int_\Omega q(\nabla\cdot \mathbf{u})\, d\Omega = 0, \tag{26}$$

where the test functions $\mathbf{w}$ and q are the sets

$$\begin{aligned} \mathbf{w} = (w_x, w_y) = h_n(x)\, h_m(y), \qquad & 0 < n, m < N \text{ Dirichlet boundary conditions} \\ & 0 \leqslant n, m \leqslant N \text{ Neumann boundary conditions} \\ q = L_n(x)\, L_m(y), \qquad & 0 \leqslant n, m \leqslant N-2, \end{aligned} \tag{27}$$

excluding the mode corresponding to the constant pressure mode in (27), $L_0(x)\, L_0(y)$. Integrating (25) by parts, we obtain

$$\int_\Omega (\nabla w_x \cdot \nabla u + \nabla w_y \cdot \nabla v)\, d\Omega + \int_S \mathbf{w}\cdot \partial \mathbf{u}/\partial n\, dS$$

$$-\int_\Omega \nabla\cdot \mathbf{w} p\, d\Omega + \int_S \mathbf{w} p\cdot \mathbf{n}\, dS = \int_\Omega \mathbf{f}\cdot \mathbf{w}\, d\Omega. \tag{28}$$

The boundary integrals vanish for the Dirichlet problem, on which we now concentrate.

We substitute (21)–(23) and (27) into (26) and (28). Discretization of the term $\int_\Omega \nabla w_x \cdot \nabla u\, d\Omega$ for one test function $h_i(x)\, h_j(y)$ results in

$$\int_{-1}^{1}\int_{-1}^{1} (h'_i(x)\, h_j(y)\, h'_k(x)\, h_l(y) + h_i(x)\, h'_j(y)\, h_k(x)\, h'_l(y))\, dx\, dy\, u_{kl}, \tag{29}$$

where primed quantities refer to differentiation and repeated indices imply summation. We obtain similar terms for $\int_\Omega \nabla w_y \cdot \nabla v\, d\Omega$. Discretization of the term $\int_\Omega \partial w_x/\partial x p\, d\Omega$ from (28) for one test function $h_i(x)\, h_j(y)$ results in

$$\int_{-1}^{1}\int_{-1}^{1} h'_i(x)\, h_j(y)\, L_k(x)\, L_l(y)\, dx\, dy\, p_{kl}. \tag{30}$$

For the other pressure term and the continuity terms we obtain terms similar to

(30). Discretization of the forcing function term $\int_\Omega f_x w_x \, d\Omega$ from (28) for one test function $h_i(x)\, h_j(y)$ results in

$$\int_{-1}^{1} \int_{-1}^{1} h_i(x)\, h_j(y)\, h_k(x)\, h_l(y)\, dx\, dy\, f_{kl}, \tag{31}$$

and we obtain similar results for the y-component of the forcing function term.

To evaluate the integrals in (29)–(31), we use Gauss–Lobatto quadrature. The quadrature points x_j are the roots of $(1-x^2)\, L'_N(x)$, and the weights are [7]

$$\omega_i = \frac{2}{N(N+1)[L_N(x_i)]^2}, \qquad i = 0, ..., N. \tag{32}$$

For future discussion, we define the inner product (Gauss–Lobatto quadrature)

$$(\phi, \psi)_{\mathrm{GL}} = \sum_{i=0}^{N} \sum_{j=0}^{N} \phi(x_i, y_j)\, \psi(x_i, y_j)\, \omega_i \omega_j. \tag{33}$$

With this quadrature, (29) becomes

$$\tilde{A}_{ijkl} u_{kl}, \tag{34}$$

where

$$\tilde{A}_{ijkl} = A_{ik} B_{jl} + A_{jl} B_{ik} \tag{35}$$

and

$$A_{nm} = \sum_{q=0}^{N} \omega_q h'_n(x_q)\, h'_m(x_q) \tag{36}$$

$$B_{nm} = \omega_n \delta_{nm}. \tag{37}$$

Term (30) becomes

$$\tilde{C}_{ijkl} p_{kl}, \tag{38}$$

where

$$\tilde{C}_{ijkl} = C_{ik} \omega_j L_l(y_j) \tag{39}$$

and

$$C_{nm} = \sum_{q=0}^{N} \omega_q h'_n(x_q)\, L_m(x_q). \tag{40}$$

Term (31) becomes

$$\tilde{B}_{ijkl} f_{kl}, \tag{41}$$

where

$$\tilde{B}_{ijkl} = B_{ik} B_{jl}. \tag{42}$$

The derivatives $h_j'(x_i)$ are given by [16]

$$\frac{dh_j}{dx}(x_i) = \begin{cases} \dfrac{L_N(x_i)}{L_N(x_j)(x_i - x_j)} & i \neq j \\ 0 & i = j \neq 0, N \\ -\dfrac{N(N+1)}{4} & i = j = 0 \\ \dfrac{N(N+1)}{4} & i = j = N. \end{cases}$$

Finally, the matrix equations corresponding to x-momentum, y-momentum, and continuity become

$$\tilde{A}_{ijkl} u_{kl} - \tilde{C}_{ijkl} p_{kl} = \tilde{B}_{ijkl} f_{x_{kl}} \tag{43}$$

$$\tilde{A}_{ijkl} v_{kl} - \tilde{C}_{jilk} p_{kl} = \tilde{B}_{ijkl} f_{y_{kl}} \tag{44}$$

$$-\tilde{C}_{klij} u_{kl} - \tilde{C}_{lkji} v_{kl} = 0 \tag{45}$$

(formulation 9, denoted by $\circ$). We can also write these equations as

$$\begin{aligned} \mathbf{A}\mathbf{u}_i - \mathbf{C}_i^{\mathrm{T}} \mathbf{p} &= \mathbf{B}\mathbf{f}_i \\ -\mathbf{C}_i \mathbf{u}_i &= 0. \end{aligned} \tag{46}$$

Here, $\mathbf{A}$ is constructed from elements $\tilde{A}_{ijkl}$, $\mathbf{C}_1$ is constructed from elements $\tilde{C}_{klij}$, and $\mathbf{C}_2$ is constructed from elements $\tilde{C}_{lkji}$ (subscripts $i = 1, 2$ represent x, y components), T stands for transpose (where, for instance, the $klij$th entry of $\mathbf{C}_1^{\mathrm{T}}$ is $\tilde{C}_{ijkl}$), and $\mathbf{B}$ is constructed from elements $\tilde{B}_{ijkl}$.

At this point it should be noted that Gauss–Lobatto quadrature is exact for polynomials up to degree $2N-1$ [7]. Therefore, the integration of the pressure and continuity terms from (26) and (28) is exact (since the polynomials are at most of degree $2N-2$; see (30)). The integration of the remaining terms, however, is inexact (since the polynomials are at most of degree $2N$; see (29) and (31)).

The main difference between the method described above and the method advanced in [9, 16] is in the form of the pressure approximation. In [9, 16] the more typical Lagrangian interpolants for pressure are used, based on the roots $\tilde{x}_j$ of the $(N-1)$th Legendre polynomial

$$p = \sum_{n=0}^{N-2} \sum_{m=0}^{N-2} p_{nm} \tilde{h}_n(x) \tilde{h}_m(y), \tag{47}$$

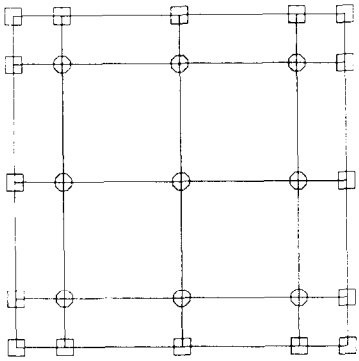

$N = 4$

Formulation No. 1

$$u = \sum_{n=0}^{N}\sum_{m=0}^{N} u_{nm}T_n(x)T_m(y)$$

$$v = \sum_{n=0}^{N}\sum_{m=0}^{N} v_{nm}T_n(x)T_m(y)$$

$$p = \sum_{n=0}^{N}\sum_{m=0}^{N} p_{nm}T_n(x)T_m(y)$$

□ = velocities specified, continuity enforced
○ = both momentum equations and continuity enforced

Formulation No. 3

$$u = \sum_{n=0}^{N}\sum_{m=0}^{N} u_{nm}T_n(x)T_m(y)$$

$$v = \sum_{n=0}^{N}\sum_{m=0}^{N} v_{nm}T_n(x)T_m(y)$$

$$p = \sum_{n=0}^{N-2}\sum_{m=0}^{N-2} p_{nm}T_n(x)T_m(y)$$

□ = velocities specified
○ = both momentum equations and continuity enforced

Formulation No. 2

$$u = \sum_{n=0}^{N}\sum_{m=0}^{N} u_{nm}T_n(x)T_m(y)$$

$$v = \sum_{n=0}^{N}\sum_{m=0}^{N} v_{nm}T_n(x)T_m(y)$$

$$p = \sum_{n=0}^{N}\sum_{m=0}^{N} p_{nm}T_n(x)T_m(y)$$

□ = velocities specified, normal momentum equation enforced
○ = both momentum equations and continuity enforced

Formulation No. 7

$$u = \sum_{n=0}^{N}\sum_{m=0}^{N} u_{nm}T_n(x)T_m(y)$$

$$v = \sum_{n=0}^{N}\sum_{m=0}^{N} v_{nm}T_n(x)T_m(y)$$

$$p = \sum_{n=0}^{N}\sum_{m=0}^{N} p_{nm}T_n(x)T_m(y)$$

□ = velocities specified, both momentum equations and continuity enforced
○ = both momentum equations and continuity enforced

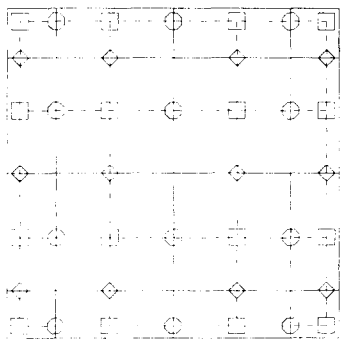

Formulation No. 4, $N = 4$

$$u = \sum_{n=0}^{N-2}\sum_{m=0}^{N-1} u_{nm}T_n(x)T_m(y)(1-x^2)(1-y^2)$$

$$v = \sum_{n=0}^{N-1}\sum_{m=0}^{N-2} v_{nm}T_n(x)T_m(y)(1-x^2)(1-y^2)$$

$$p = \sum_{n=0}^{N-1}\sum_{m=0}^{N-1} p_{nm}T_n(x)T_m(y)$$

□ = continuity enforced
○ = x-momentum equation enforced
◇ = y-momentum equation enforced

FIG. 1. Grids for formulations 1–7, 9, 10 (formulation 8 is similar to formulation 3 with Legendre polynomials replacing Chebyshev polynomials).

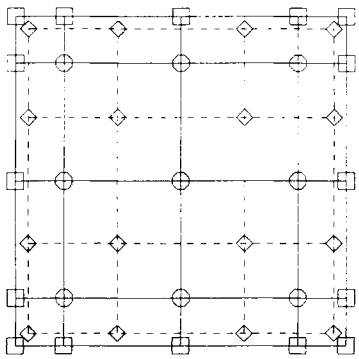

Formulation No. 5, $N = 4$

$$u = \sum_{n=0}^{N}\sum_{m=0}^{N} u_{nm}T_n(x)T_m(y)$$

$$v = \sum_{n=0}^{N}\sum_{m=0}^{N} v_{nm}T_n(x)T_m(y)$$

$$p = \sum_{n=0}^{N-1}\sum_{m=0}^{N-1} p_{nm}T_n(x)T_m(y)$$

□ = velocities specified
○ = both momentum equations enforced
◇ = continuity enforced

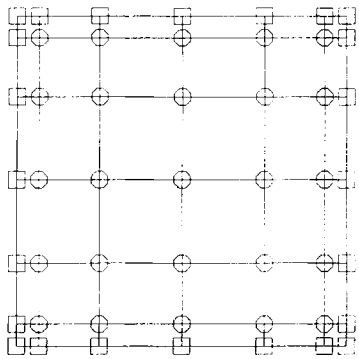

Formulation No. 6, $N = 4$, $M = 6$

$$u = \sum_{n=0}^{N}\sum_{m=0}^{N} u_{nm}T_n(x)T_m(y)$$

$$v = \sum_{n=0}^{N}\sum_{m=0}^{N} v_{nm}T_n(x)T_m(y)$$

$$p = \sum_{n=0}^{N}\sum_{m=0}^{N} p_{nm}T_n(x)T_m(y)$$

□ = velocities specified
○ = both momentum equations and continuity enforced

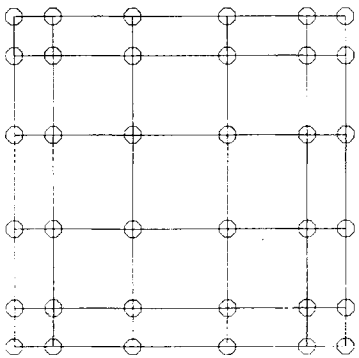

Formulation No. 9, $N = 5$

$$u = \sum_{n=0}^{N}\sum_{m=0}^{N} u_{nm}h_n(x)h_m(y)$$

$$v = \sum_{n=0}^{N}\sum_{m=0}^{N} v_{nm}h_n(x)h_m(y)$$

$$p = \sum_{n=0}^{N-2}\sum_{m=0}^{N-2} p_{nm}L_n(x)L_m(y)$$

○ = velocities defined

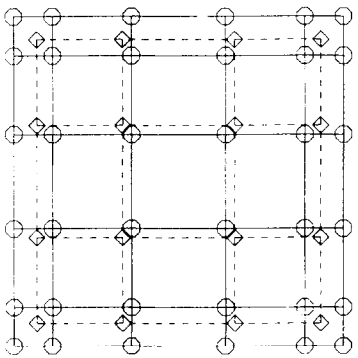

Formulation No. 10, $N = 5$

$$u = \sum_{n=0}^{N}\sum_{m=0}^{N} u_{nm}h_n(x)h_m(y)$$

$$v = \sum_{n=0}^{N}\sum_{m=0}^{N} v_{nm}h_n(x)h_m(y)$$

$$p = \sum_{n=0}^{N-2}\sum_{m=0}^{N-2} p_{nm}\tilde{h}_n(x)\tilde{h}_m(y)$$

○ = velocities defined
◇ = pressure defined

FIG. 1—*Continued*

where

$$\tilde{h}_j(x) = \frac{L_{N-1}(x)}{L'_{N-1}(\tilde{x}_j)(x - \tilde{x}_j)}, \qquad j = 0, ..., N-2. \tag{48}$$

Equation (48) is derived in a manner similar to the derivation of (24). The unknowns p_{nm} in (47) are the values of pressure on the Gauss–Legendre grid points $(\tilde{x}_n, \tilde{y}_m)$ defined below. The test function q is given similarly,

$$q = \tilde{h}_n(x)\,\tilde{h}_m(y), \qquad 0 \leqslant n, m \leqslant N-2, \tag{49}$$

excluding one particular test function $\tilde{h}_n(x)\,\tilde{h}_m(y)$ corresponding to the pressure specified at point (x_n, y_m). We now define a Gauss–Legendre quadrature based on the roots $\tilde{x}_i$ of the $(N-1)$th Legendre polynomial (the roots are not known in closed form):

$$(\phi, \psi)_G = \sum_{i=0}^{N-2} \sum_{j=0}^{N-2} \phi(\tilde{x}_i, \tilde{y}_j)\,\psi(\tilde{x}_i, \tilde{y}_j)\,\rho_i \rho_j. \tag{50}$$

The weights are [7]

$$\rho_i = \frac{2}{(1 - \tilde{x}_i^2)[L'_{N-1}(\tilde{x}_i)]^2}, \qquad i = 0, ..., N-2. \tag{51}$$

The discrete problem then becomes

$$\begin{aligned} (\nabla \mathbf{u}, \nabla \mathbf{w})_{GL} - (\nabla \cdot \mathbf{w}, p)_G &= (\mathbf{w}, \mathbf{f})_{GL} \\ -(q, \nabla \cdot \mathbf{w})_G &= 0 \end{aligned} \tag{52}$$

(formulation 10, denoted by □). We compare this with our formulation (○):

$$\begin{aligned} (\nabla \mathbf{u}, \nabla \mathbf{w})_{GL} - (\nabla \cdot \mathbf{w}, p)_{GL} &= (\mathbf{w}, \mathbf{f})_{GL} \\ -(q, \nabla \cdot \mathbf{w})_{GL} &= 0. \end{aligned} \tag{53}$$

The difference between the two methods lies in the pressure approximation and type of quadrature for the pressure and continuity terms. Note that the pressure and continuity terms in (52) involve inexact quadratures. The Gauss–Legendre quadrature is exact for polynomials up to order $2N-3$, while (52) contains polynomials of degree $2N-2$. The operation count for construction of the matrix elements is slightly higher for (53) due to the terms C_{nm} from (40); however, the number of operations to set up the matrices for both methods is $O(N^4)$, compared to $O(N^6)$ for direct solution of the algebraic system.

In our method (53), we remove the constant pressure mode by setting $p_{00} = 0$,. For the method described by (52) we set the pressure equal to zero at one point on the Gauss–Legendre grid. Figure 1 shows the grids and approximations for all the formulations.

3. Corner Singularities

The presence of corner singularities destroys the accuracy of spectral methods. To restore the accuracy, we use a method that "subtracts" the singularity [18]. We consider the driven cavity problem where inertial effects are neglected (Reynolds number equal to zero), which is defined by the Stokes equations (3) and (4), $-1 \leqslant x, y \leqslant 1$, where $\mathbf{f} = 0$. The boundary conditions are $u(x, 1) = -1$; all other boundary velocities are equal to zero. At the top corners $(x, y) = (-1, 1)$ and $(1, 1)$, u is multivalued, resulting in a singular solution.

We decompose each of our variables into a computational and singular solution:

$$\begin{aligned} u &= u_c + u_s \\ v &= v_c + v_s \\ p &= p_c + p_s. \end{aligned} \tag{54}$$

The singular solution for viscous flow in the upper right corner with one moving wall is [1] (see Fig. 2)

$$\begin{aligned} u_{s_1} &= \frac{-1}{1-\pi^2/4}\left[(1-\pi^2/4)\cos\theta + (\pi/2)\theta\cos\theta + (\pi/2)\sin\theta - \theta\sin\theta\right] \\ v_{s_1} &= \frac{1}{1-\pi^2/4}\left[(-\pi^2/4)\sin\theta + (\pi/2)\theta\sin\theta + \theta\cos\theta\right] \\ p_{s_1} &= \frac{2\cos\theta + \pi\sin\theta}{(1-\pi^2/4)r} + C, \end{aligned} \tag{55}$$

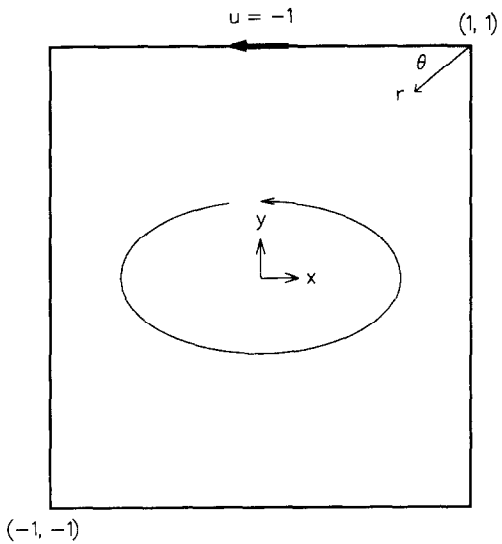

Fig. 2. Coordinate system for driven cavity.

where C is a constant of integration. We do not take advantage of the symmetries of this problem; therefore we must add the singular solutions for the upper left corner (u_{s_2}, v_{s_2}, and p_{s_2}) to the solutions given above to obtain

$$u_{s_1} + u_{s_2} = u_s \tag{56}$$

and likewise for v_s and p_s. Substituting (54) into the governing equations (3) and (4) and recognizing that (56) is a solution to (3) and (4), we obtain the computational problem

$$\begin{aligned} \nabla^2 \mathbf{u}_c - \nabla p_c &= 0 \\ \nabla \cdot \mathbf{u}_c &= 0, \end{aligned} \tag{57}$$

with boundary conditions $u_c(x, 1) = -1 - u_s(x, 1)$, $v_c(x, 1) = -v_s(x, 1)$, and $u_c = -u_s$, $v_c = -v_s$ elsewhere on the boundary. Note that computationally we must specify only one u value in the upper corners where analytically the velocity is multivalued. It does not matter what value we choose for u in the upper corners, as long as we assign the corresponding value to the singular form u_s (since u_s can take on any value in the upper corners, being only dependent on θ, we must assign it some value prior to adding it to the computational solution u_c). We set the constant pressure mode equal to zero for our formulation, and for the method described by (52), we set $p_c = -p_s$ at a point in the flow.

We can solve (57) using any of the techniques described previously (although implementation of formulation 4 would be difficult due to the inhomogeneous boundary conditions).

4. Results and Comparisons

We solve three test problems using the formulations in Section 2: a problem with an exact solution, a problem with homogeneous boundary conditions, and the driven cavity problem. The domain for all problems is $-1 \leqslant x, y \leqslant 1$. In the following comparisons, the RMS error is calculated on a 31×31 uniform grid, including the boundaries. The solutions are compared to an "exact" solution (which in some cases corresponds to one of the formulations described in Section 2 with a high truncation). The velocity errors are the combined RMS errors for both u and v. Note that formulations resulting in singular matrices are solved using standard matrix solvers (solutions are only obtained because roundoff error in the matrix decomposition process results in no pivots exactly equal to zero).

Formulation with exact solution. First, we solve (3) and (4) with

$$\mathbf{f} = (2 + \pi \cos \pi x \sin \pi y, \pi \sin \pi x \cos \pi y)$$

and the boundary conditions $\mathbf{u} = (1 - y^2, 0)$. This problem, suggested by Ronquist

in [16], has the exact solution $\mathbf{u} = (1 - y^2, 0)$ and $p = \sin \pi x \sin \pi y$. Figures 3 and 4 show the convergence of the velocities and pressure for the formulations described in Section 2 to the exact solution as a function of the number of degrees of freedom for one velocity component in one direction (in other words, $N+1$). (The fully staggered formulation is not shown because it requires homogeneous boundary conditions.) Several comments are in order:

1. The overdetermined collocation formulation ($\diamond$) converges fastest. The weak formulation using Lagrangian interpolants for pressure ($\square$) converges slowest.

2. All formulations show a stepwise convergence where the increase in accuracy in going from odd N to even N is less than the increase in accuracy in going from even N to odd N. The exact solution for velocity is symmetric in x and y, and the exact solution for pressure is antisymmetric in both directions. We suspect that the pressure computation dominates the solution accuracy so that the addition of an even basis function does not significantly increase the solution accuracy. This conjecture is substantiated by the driven cavity results where there are no symmetries in the y-direction and the solutions converge with less of a stepwise behavior.

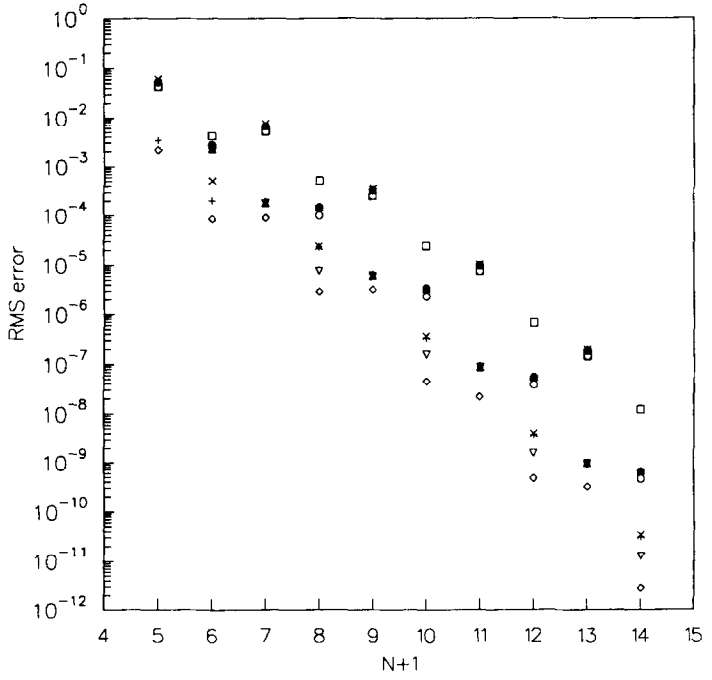

FIG. 3. Problem with exact solution—velocity error.

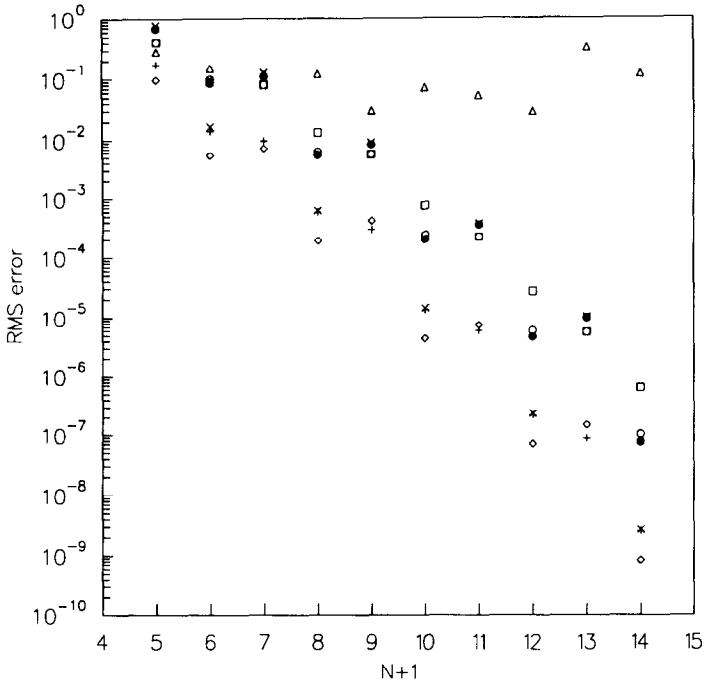

FIG. 4. Problem with exact solution—pressure error.

3. As mentioned in Section 2.1, the formulation where continuity is enforced on the boundary (∇) leads to singular matrices. The pressure solution is therefore on the order of the inverse of machine accuracy (10^{+15}), but the velocity solution is accurate (Bernardi, Canuto, and Maday [5] show that the existence of spurious pressure modes does not pollute the velocity solution).

4. The semi-staggered grid formulation ($\triangle$) also results in singular matrices, but the pressure solution is accurate to about 10^{-1}. This accuracy, however, is far poorer than that of the other methods.

5. The most oscillatory convergence behavior is given by the formulation where the normal momentum equation is enforced on the boundary ($\times$).

6. The most linear convergence (i.e., the smallest fluctuations about the best-fit straight line on a semi-log plot as N increases) is given by the method where the system is overdetermined by enforcing the continuity and x- and y-momentum equations on the boundary ($+$) and by the weak formulation using Lagrangian interpolants for pressure ($\square$).

Homogeneous boundary conditions. The second test problem is one with homogeneous boundary conditions. Equations (3) and (4) are solved with $\mathbf{f} = (0, -x)$. The solution for u is symmetric in x and antisymmetric in y, the solution

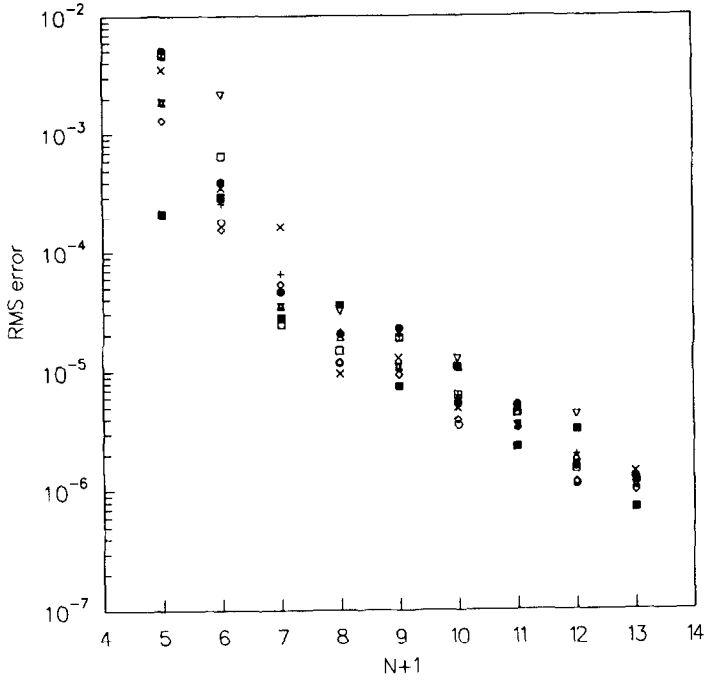

FIG. 5. Problem with homogeneous boundary conditions—velocity error.

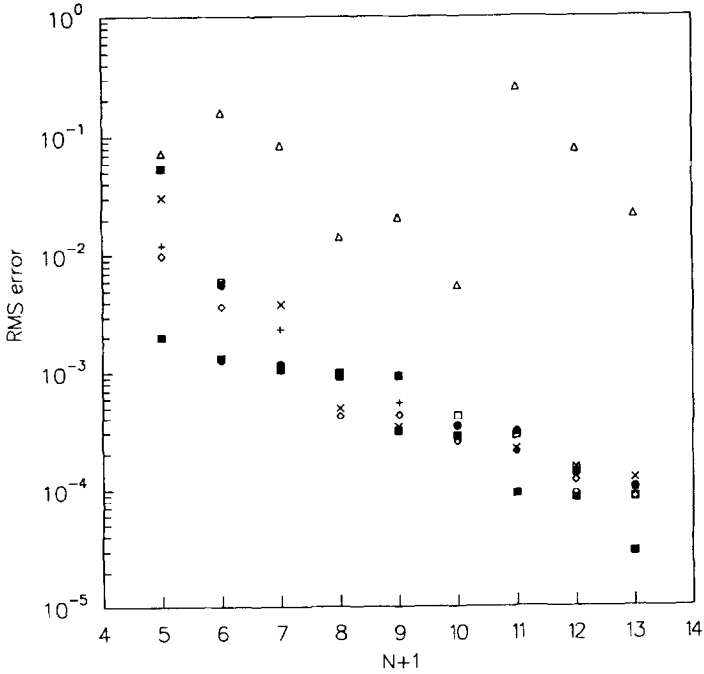

FIG. 6. Problem with homogeneous boundary conditions—pressure error.

for v is antisymmetric in x and symmetric in y, and the solution for pressure is antisymmetric in x and y. For this problem, all formulations are evaluated against the solution from the fully staggered formulation (which satisfies the boundary conditions exactly) at $N=20$. The RMS difference between results for the fully staggered formulation for $N=18$ and $N=20$ is 2.15×10^{-8} for velocity and 7.69×10^{-7} for pressure. The convergence is shown in Fig. 5 and 6, and we note several observations:

1. The stepwise convergence behavior of the different methods is less conspicuous than for the case with the exact solution, except that the fully staggered method (■) oscillates from best to worst.

2. The method with continuity applied on the boundary (▽, singular system) gives the worst results.

3. Again, the semi-staggered formulation (△) pressure solution is accurate to about 10^{-1}, despite the singular matrix. This accuracy is far poorer than that of the other methods.

Driven cavity. The third test problem is Stokes flow in a driven cavity. The corner singularities are treated as described in Section 3. For this problem, all formulations (except the fully staggered formulation ■, which does not readily admit

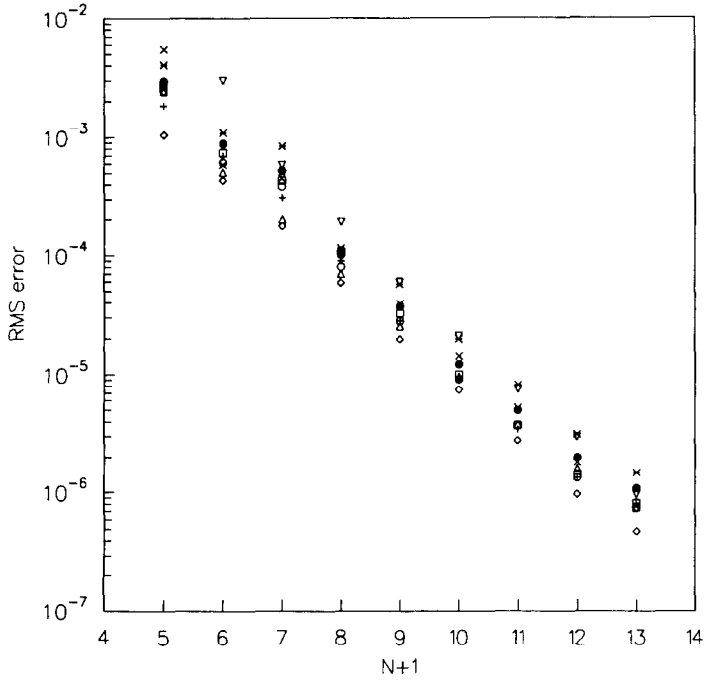

FIG. 7. Driven cavity—velocity error.

inhomogeneous boundary conditions) are compared to an "exact" solution from the formulation where the system is determined by enforcing the normal momentum equation on the boundary ($\times$). We choose this formulation (with $N=19$) for our "exact" solution because is the formulation with a determined system which gives the best convergence (for odd N) for the test problem with the exact solution. The overdetermined formulations gave better convergence (in the RMS sense) for the same test problem, but they do not satisfy the boundary conditions as well. The RMS difference between results for the formulation where the normal momentum equation is enforced on the boundary for $N=17$ and $N=19$ is 1.21×10^{-8} for velocity and 1.06×10^{-5} for pressure.

The convergence is shown in Figs. 7 and 8. Table II lists the values of velocity and pressure for the "exact" solution at various locations in the cavity. Note that the pressure is singular in the upper corners, and hence these two points are avoided in the computation of RMS pressure error. We note the following:

1. The accuracy of the different methods varies less than for the case with the exact solution, and the convergence for all methods is nearly monotonic (except for pressure for the semi-staggered formulation, $\triangle$).

2. The semi-staggered formulation ($\triangle$) gave $O(10^{-1})$ pressure error for odd N and O (machine roundoff)$^{-1}$ error for even N.

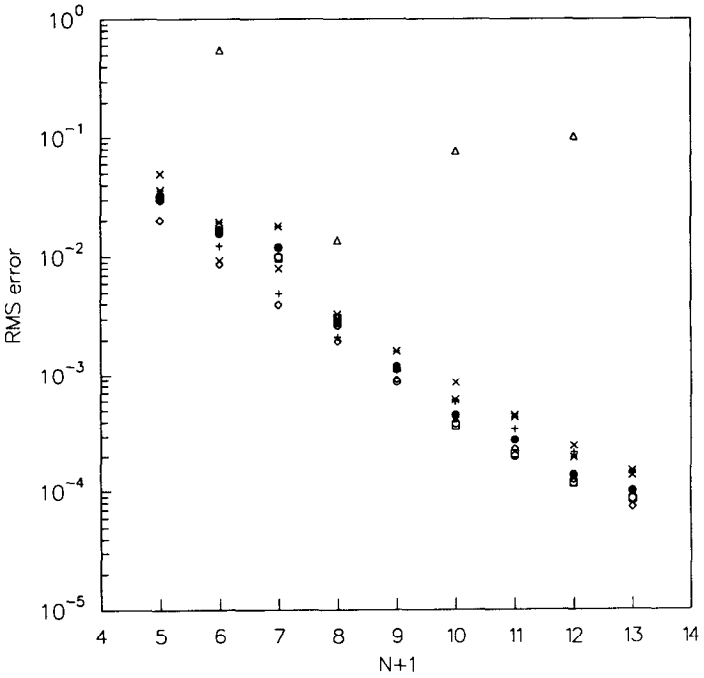

FIG. 8. Driven cavity—pressure error.

TABLE II

"Exact" Solution to the Driven Cavity with Re = 0

Y/X	-1	.8	.6	.4	.2	0
1	-1.0000000	-1.0000000	-1.0000000	-1.0000000	-1.0000000	-1.0000000
.8	0.0000000	0.0387091	-0.1941371	-0.3581729	-0.4409777	-0.4659723
.6	0.0000000	0.0777508	0.0720573	-0.0047757	-0.0675273	-0.0898410
.4	0.0000000	0.0579981	0.1216621	0.1340484	0.1230553	0.1164180
.2	0.0000000	0.0433758	0.1162892	0.1673256	0.1908748	0.1970266
0	0.0000000	0.0328053	0.0977599	0.1566186	0.1931996	0.2051917
-.2	0.0000000	0.0245499	0.0771044	0.1302338	0.1669410	0.1797918
-.4	0.0000000	0.0177414	0.0574571	0.1001258	0.1312854	0.1425564
-.6	0.0000000	0.0115595	0.0388143	0.0698032	0.0934047	0.1021317
-.8	0.0000000	0.0050785	0.0196663	0.0378941	0.0523472	0.0577765
-1	0.0000000	0.0000000	0.0000000	0.0000000	0.0000000	0.0000000

X-velocity—symmetric in x

Y/X	-1	.8	.6	.4	.2	0
1	0.0000000	0.0000000	0.0000000	0.0000000	0.0000000	0.0000000
.8	0.0000000	-0.3372808	-0.1603051	-0.0746074	-0.0304259	0.0000000
.6	0.0000000	-0.3573925	-0.3016425	-0.1809661	-0.0821167	0.0000000
.4	0.0000000	-0.2775081	-0.3064999	-0.2209680	-0.1104230	0.0000000
.2	0.0000000	-0.1997354	-0.2516495	-0.2028153	-0.1085414	0.0000000
0	0.0000000	-0.1356660	-0.1841155	-0.1586910	-0.0888056	0.0000000
-.2	0.0000000	-0.0854321	-0.1221699	-0.1100791	-0.0634484	0.0000000
-.4	0.0000000	-0.0475987	-0.0717330	-0.0669863	-0.0394511	0.0000000
-.6	0.0000000	-0.0209111	-0.0341098	-0.0330275	-0.0197929	0.0000000
-.8	0.0000000	-0.0050363	-0.0095694	-0.0096214	-0.0058372	0.0000000
-1	0.0000000	0.0000000	0.0000000	0.0000000	0.0000000	0.0000000

Y-velocity—antisymmetric in x

Y/X	-1	.8	.6	.4	.2	0
1	-----	5.1481999	1.8643627	0.8425649	0.3431065	0.0000000
.8	8.9486277	7.0477570	3.2223647	1.5174802	0.6246027	0.0000000
.6	3.4836682	3.8638592	2.6560704	1.5111069	0.6742606	0.0000000
.4	1.6264834	2.0688288	1.7557603	1.1648138	0.5646678	0.0000000
.2	0.7385006	1.1053392	1.0714049	0.7904395	0.4088965	0.0000000
0	0.2844696	0.5743197	0.6276939	0.5019346	0.2727323	0.0000000
-.2	0.0707722	0.2926206	0.3653628	0.3131434	0.1769433	0.0000000
-.4	0.0040980	0.1659230	0.2307103	0.2083681	0.1212649	0.0000000
-.6	0.0329371	0.1385820	0.1853848	0.1697231	0.1002944	0.0000000
-.8	0.1174415	0.1693917	0.2051417	0.1873981	0.1115402	0.0000000
-1	0.1681224	0.2179560	0.2849620	0.2677581	0.1606348	0.0000000

Pressure—antisymmetric in x

3. The pseudospectral formulation where the order of the pressure approximation is two less than that of velocity gives slightly poorer results when we use a Legendre expansion (∗), rather than a Chebyshev expansion (•).

Figure 9 shows how the velocity and pressure convergence to the "exact" solution with and without the singular function separated from the computational solution. We make these comparisons using the weak formulation method with pressure approximated by a Legendre expansion (formulation 9). The subtraction of the singularity greatly improves the accuracy of the solution.

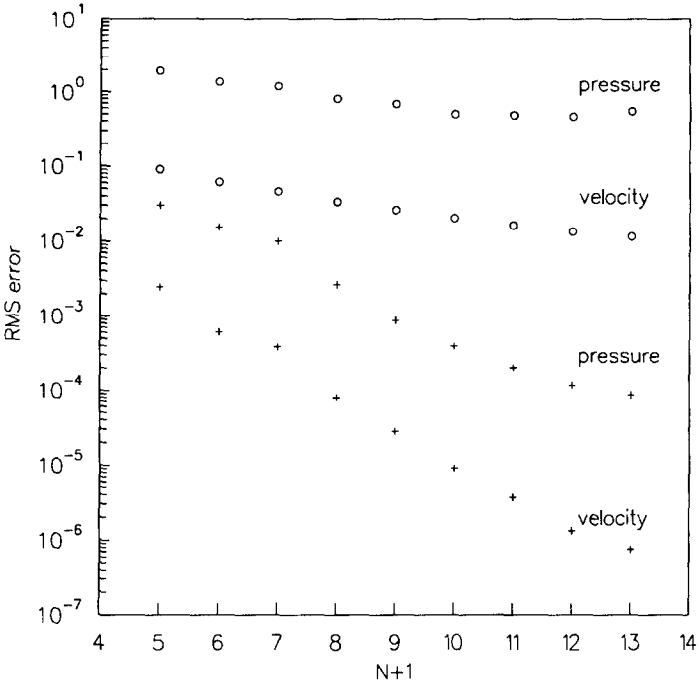

FIG. 9. Velocity and pressure error for driven cavity problem with and without special treatment for strongest corner singularities: ◦ without spectial treatment; + with special treatment.

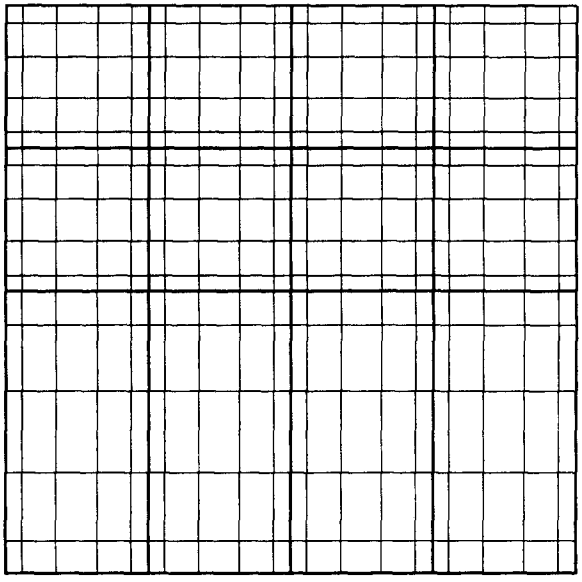

FIG. 10. Multi-element domain (shown with $N = 5$).

We now present some results for the driven cavity problem using the multi-element domain shown in Fig. 10. We use the weak formulations in our multi-element approach, following the work of Maday and Patera [9] and Ronquist [16]. Communication between elements is established through the conventional finite element direct stiffness summation approach, which matches velocities at the nodal values. Maday and Patera [9] show that velocity gradients are weakly continuous at element interfaces. The domain is divided into 12 elements, four of which are not square. We choose this decomposition to show the potential of the weak formulations to handle more complicated geometries and to observe how the decomposition isolates the upper corner singularities. Figures 11 and 12 show the convergence of the two weak formulations ($\circ$ and $\square$) with the number of degrees of freedom $N+1$ in each element using the special treatment of the upper corner singularities as described in Section 3. Our formulation ($\circ$) gives slightly better accuracy than the weak formulation with Lagrangian interpolants for pressure ($\square$). We suspect this improvement is due to our exact quadrature of the continuity terms (see Section 2.2). Figure 13 shows how the special treatment of the singularities affects the accuracy of formulation 9. Accuracy is improved by a factor of a hundred or more.

Here we briefly address the domain decomposition approach for isolation of corner singularities where singular functions are not subtracted. Figure 14 shows how

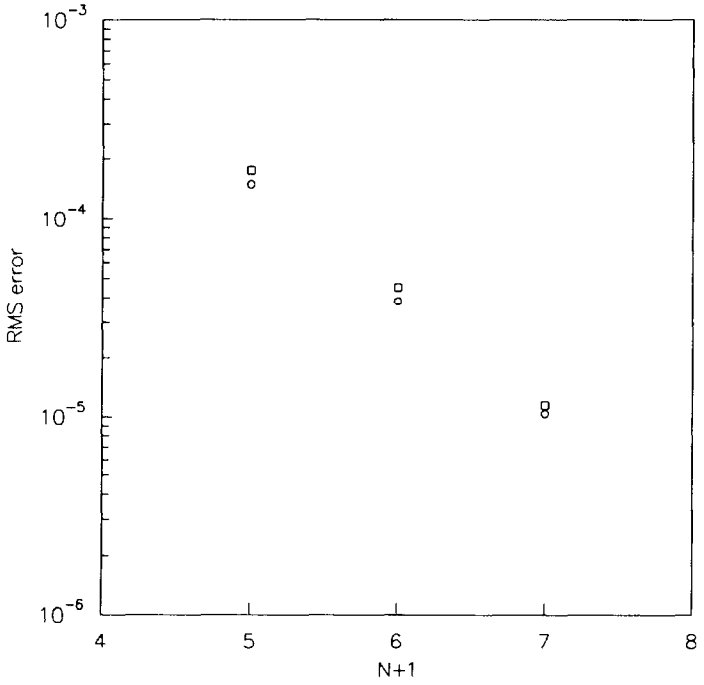

FIG. 11. Multi-element domain—driven cavity problem—velocity error.

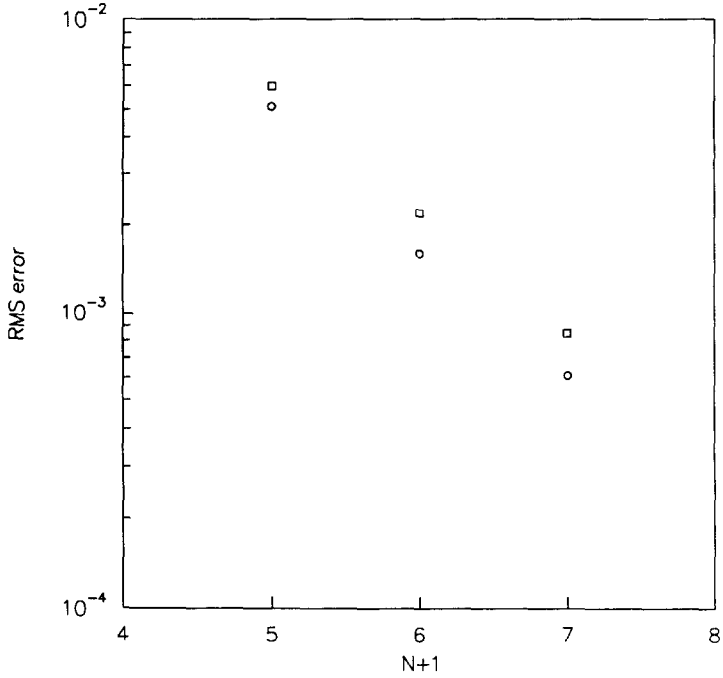

FIG. 12. Multi-element domain—driven cavity problem—pressure error.

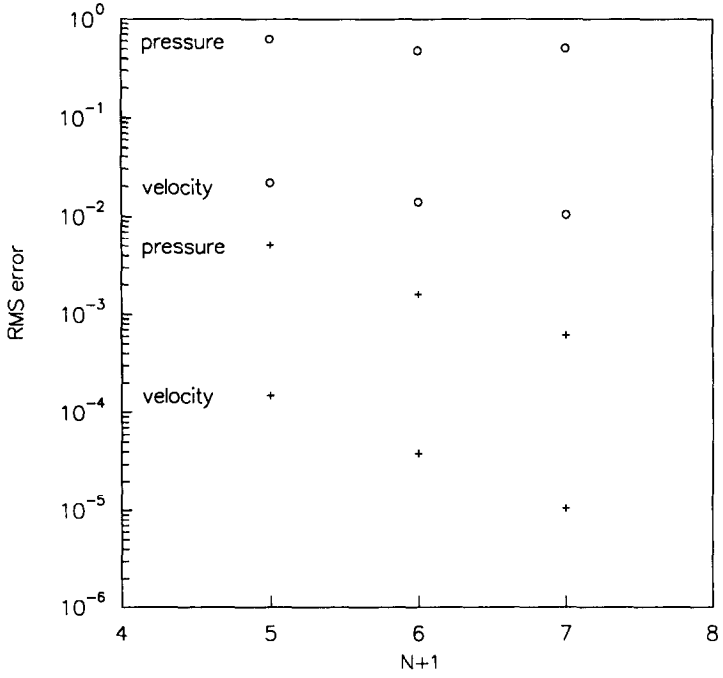

FIG. 13. Multi-element domain—velocity and pressure errors for driven cavity problem with and without special treatment for strongest corner singularities: ◦ without special treatment; + with special treatment.

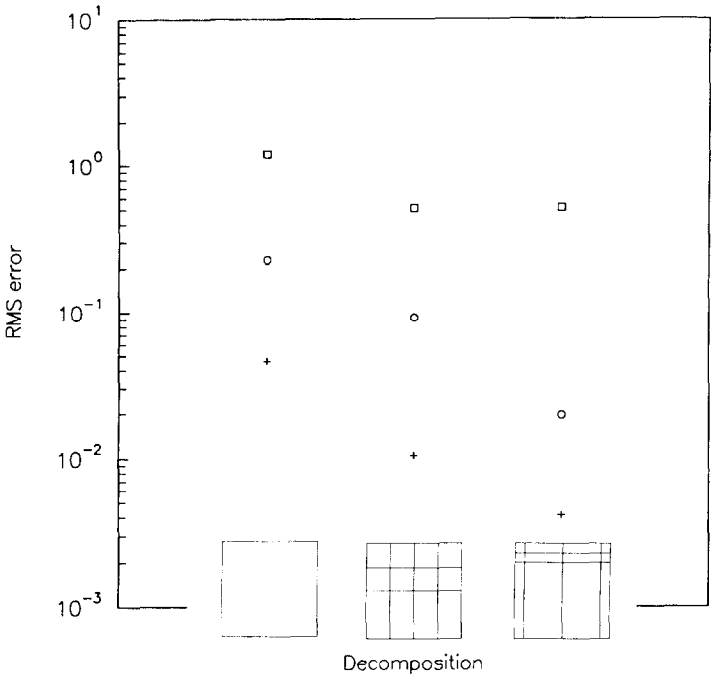

FIG. 14. Velocity and pressure errors for driven cavity problem for different domain decompositions, $N=6$ in each element: □ pressure error for entire uniform grid; ◦ pressure error excluding top near-corner grid points; + velocity error.

velocity and pressure errors vary as the domain decomposition is changed (using our formulation ◦, number 9). The truncation is $N=6$ in each direction for each element for all the decompositions shown. As expected, the velocity solutions improve as the number of elements increases. Also, making the upper corner elements smaller further improves the solutions. The pressure error convergence, however, is not remarkable when the RMS error is calculated using all the uniform grid points (denoted by □ in the figure). The magnitude of the error is governed by the pressures on the uniform grid in the vicinity of the upper corners, which are typically $O(10)$. Since the polynomial expansion has the most difficulty resolving the solution in the upper corners, and since this error dominates the RMS calculation, the plotted pressure errors show particularly poor convergence. However, if we neglect a number of points in the vicinity of the upper corners for the error calculation we find that convergence is improved. The symbol ◦ denotes the pressure error when we neglect a square region $y > 0.734$, $|x| > 0.734$ in each of the top corners. These results demonstrate, as expected, that domain decomposition can be viable alternative for isolation of corner singularities. However, a single element domain where the singular functions are subtracted is preferable to solely a domain decomposition approach.

5. Computational Complexity

The solution times for the weak formulations are much shorter than for the pseudospectral methods, because the weak formulations can use a symmetric matrix solver while the pseudospectral methods cannot. Gaussian elimination routines were exclusively used in this study. To indicate the relative solution times for the driven cavity problem, we plot in Fig. 15 the RMS velocity error versus total matrix size (rows × columns). The abscissa values for the weak formulations are shown as the total matrix size divided by two, since the symmetric matrix solver takes approximately half the time of a non-symmetric matrix Gaussian elimination routine. For any given matrix size it is seen that the single-element weak formulations (○ and □) provide much better accuracy than any of the pseudospectral methods. We also plot in Fig. 15 the multi-element results for formulation 9 (we distinguish this from the single-element formulation by the symbol ▲). All of the single-element formulations are vastly more accurate than the multi-element formulation for a given matrix size (sparsity of the multi-element formulation is not considered). The convergence rate of the multi-element formulation (▲) also appears slower than that of the single-element weak formulations (○ and □). For the results shown in Fig. 15 the singularities are treated as described in Section 3.

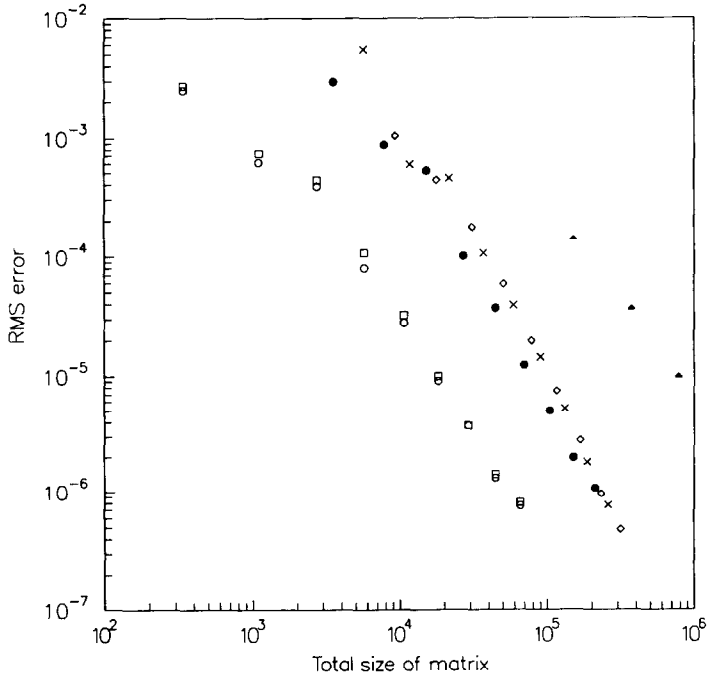

Fig. 15. Velocity error for driven cavity problem versus size of matrix—all formulations on single-element domain, except ▲: formulation 9 on multi-element domain.

The number of equations for these two-dimensional Stokes flow problems is $Q \approx 3KN^2$, where K is the number of elements. Gaussian elimination provides a solution in $O(Q^3)$ operations. For large N or K, Gaussian elimination becomes impractical. Iterative solutions of the linear systems, involving matrix–vector multiplications of $O(N^3)$ operations per element, are necessary for problems with higher truncation or larger numbers of elements.

Although the pseudospectral method is relatively easy to formulate and program, both weak formulations have the advantage that the matrices **A** and **C** from (46) are positive-definite. Ronquist [16] describes how this feature can be used in the iterative solution of large systems.

6. Conclusions

We have shown via several test problems that staggered grids are not necessary to eliminate spurious pressure modes in spectral methods where the Stokes equations are solved directly. The matrix that results from discretization in the pseudospectral method can be made nonsingular in a variety of ways, including application of the normal momentum equation on the boundary, approximation of pressure with basis functions of order two less than those for velocity, and overdetermination. The weak formulation we present avoids the use of a staggered grid and provides accurate quadrature, while maintaining efficiency. While our discussion focuses on rectilinear single-element problems, of particular interest in future work will be the extension of our weak formulation to non-rectilinear multi-element constructions. We show that separation of the singular and computational solutions for problems with strong corner singularities restores the accuracy of spectral methods. For solution of Stokes flow in a square domain and for a given truncation N, this special treatment of corner singularities is preferable to a domain decomposition approach, both in terms of accuracy and computational speed.

Acknowledgments

This work was supported by National Science Foundation Contract DMC-8716766. We would like to thank the reviewers for helpful comments and suggestions, and also R. Akhavan for supplying material indispensable in this research.

References

1. G. K. Batchelor, *An Introduction to Fluid Dynamics* (Cambridge Univ. Press, London, 1967).
2. C. Bernardi and Y. Maday, *Int. J. Numer. Methods Fluids* **8**, 537 (1988).
3. C. Bernardi, Y. Maday, and B. Metivet, *Rech. Aerosp.* **1987**, No. 1, 1 (1987).
4. C. Bernardi, Y. Maday, and B. Metivet, *Numer. Math.* **51**, Fasc. 6, 655 (1987).
5. C. Bernardi, C. Canuto, and Y. Maday, *SIAM J. Numer. Anal.* **25**, No. 6, 1237 (1988).

6. J. P. BOYD, *Chebyshev and Fourier Spectral Methods* (Springer-Verlag, Berlin/Heidelberg, 1989).
7. C. CANUTO, M. Y. HUSSAINI, A. QUARTERONI, AND T. A. ZANG, *Spectral Methods in Fluid Dynamics* (Springer-Verlag, New York, 1988).
8. D. GOTTLIEB, M. Y. HUSSAINI, AND S. A. ORSZAG, in *Spectral Methods for Partial Differential Equations* (Soc. Indus. Appl. Math., Philadelphia, 1984).
9. Y. MADAY AND A. T. PATERA, "Spectral Element Methods for the Incompressible Navier–Stokes Equations," in *State-of-the-Art Surveys in Computational Mechanics*, edited by A. K. Noor (ASME, New York, 1988).
10. F. MONTIGNY-RANNOU AND Y. MORCHOISNE, *Int. J. Numer. Methods Fluids* 7, 175 (1987).
11. Y. MORCHOISNE, "Résolution des équations de Navier–Stokes par une méthode spectrale de sous-domaines," in *Comptes-Rendus de 3éme Congrés Int. sur les Méthodes Numériques de l'Ingénieur*, edited by P. Lascaux (L'Academie des Sci., Paris, 1983).
12. S. A. ORSZAG, M. ISRAELI, AND M. O. DEVILLE, *J. Sci. Comput.* **1**, No. 1, 75 (1986).
13. S. V. PATANKAR, *Numerical Heat Transfer and Fluid Flow* (Hemisphere, Washington, DC, 1980).
14. A. T. PATERA, *J. Comput. Phys.* **54**, 468 (1984).
15. R. PEYRET AND T. D. TAYLOR, *Computational Methods for Fluid Flow* (Springer-Verlag, New York, 1983).
16. E. M. RONQUIST, *Optimal Spectral Element Methods for the Unsteady Three-Dimensional Incompressible Navier–Stokes Equations*, Ph.D. thesis, Massachusetts Institute of Technology, 1988 (unpublished).
17. E. M. RONQUIST AND A. T. PATERA, *Int. J. Numer. Methods Eng.* **24**, 2273 (1987).
18. W. W. SCHULTZ, N. Y. LEE, AND J. BOYD, *J. Sci. Comput.* **4**, 1 (1989).
19. T. M. SHIH AND A. L. REN, *Numer. Heat Transfer* **7**, 413 (1984).